Evaluation of directional quadrature schemes for simulating urban radiative transfer using the Discrete Ordinate Method

Feng Wang, Frederic Andre, Frederic Kuznik, Etienne Vergnault

Evaluation of directional quadrature schemes for simulating urban radiative transfer using the Discrete Ordinate Method

Feng WANG[a,d], Frédéric ANDRE[b], Frédéric KUZNIK[a], Étienne VERGNAULT[c]

[a] *Univ Lyon, INSA Lyon, CNRS, CETHIL, UMR5008, 69621 Villeurbanne, France*
[b] *Univ Lyon, CNRS, INSA Lyon, CETHIL, UMR5008, 69621 Villeurbanne, France*
[c] *Univ Lyon, UCBL, INSA Lyon, CNRS, CETHIL, UMR5008, 69622 Villeurbanne, France*
[d] *Suzhou Institute of Building Science Group Co.,Ltd, SuZhou, China*

Abstract

In the last decades, different numerical methods have been applied to simulate radiative transfer in urban configurations. In cases where atmospheric air is treated as an absorbing gas, it has been shown in many cases that the use of the Discrete Ordinate Method has been shown in many situations to provide a good compromise between calculation cost and accuracy. In this paper, several quadrature schemes for directional integration in the DOM are compared for different urban conditions and types (visible, thermal infrared) of radiation. This allows for determining which angular quadrature scheme is the most appropriate for urban radiative transfer calculations. In conclusion, the Fibonacci quadrature set outperforms all other quadratures in the traditional canyon simulation with a transparent model. Meanwhile, the performance of Level Symmetric Odd and Hybrid quadrature (LSO/LSH) and Equal Weight Odd (EWO) catch up with Fibonacci's in a participative atmosphere model.

Keywords: Quadrature, Radiation, Discrete Ordinate Method, Urban Geometry

Nomenclature

α	interpolation coefficient	κ_λ	absorption coefficient
β_λ	spectral extinction coefficient	λ	wavelength
ϵ_{atm}	sky emissvity	μ_m, η_m, ξ_m	coordinates of discrete direction Ω_m
$\epsilon_{w,\lambda}$	spectral emissivity of the boundary surface at wavelength λ	Ω	radiation direction
		Ω_m	discrete direction

Email address: etienne.vergnault@insa-lyon.fr (Étienne VERGNAULT)

ω_m	discrete direction weight factor
ϕ_m	polar angle of quadrature direction m
ϕ_{golden}	m_{th} golden ratio
σ_λ	scattering coefficient
θ_m	azimuthal angle of quadrature direction m
$\zeta_x^m, \zeta_y^m, \zeta_z^m$	interpolation coefficient for the axis x,y,z
F_m	m_{th} Fibonacci number
I_λ^0	radiative intensity of blackbody
$I_\lambda(s, \Omega)$	radiative intensity in direction Ω at wavelength λ
$I_{\lambda,p,m}$	volume averaged radiative intensity
$I_{\lambda,S,m}$	interface averaged radiative intensity
I_{atm}	sky infrared radiation
$I_{b,w,\lambda}$	the blackbody intensity evaluated at the temperature of the surface element w
I_{dif}	diffused solar radiation intensity
I_{dir}	direct solar radiation intensity
I_{env}	environment infrared radiation
I_{ref}	reflected solar radiation intensity
I_{sw}	Total solar radiation intensity
n	discretization number
$P(\Omega, \Omega')$	phase function
R_1, R_2	numbers from Low Discrepancy Sequence
$T_{(s)}$	medium temperature
T_{atm}	effective sky temperature
x_{SA}, y_{SA}, z_{SA}	coordinates of curve surface centroid
x_{tri}, y_{tri}, z_{tri}	coordinates of tirangle centroid

1. Introduction

Radiation is an important part of the heat budget in thermal simulations of urban areas. Different sources of radiation (direct solar flux, infrared radiation by the walls of the buildings, etc.) together with the complex geometry encountered at the city scale have led to difficulty in calculating radiative transfer and, in most realistic cases, high costs.

Many works dedicated to radiative transfer at the building scale [1, 2, 3] use the radiosity or ray casting methods for such calculation. These techniques provide acceptable results at a reasonable computational cost. However, they all ignore the interactions between the participating atmosphere (gases and aerosols can absorb and scatter radiation) and the radiation field. In some circumstances, such as those involving polluted atmosphere, fog, rain, or high humidity, the atmosphere may exert a significant impact on radiative transfer, as dispersed species significantly increase their ability to absorb and emit radiative energy.

Numerous methods have been developed to calculate the radiative heat transfer in participating media such as the finite volume method (FVM) [4, 5], the method of lines [6], the discrete ordinate method (DOM) [7, 8], the P-N method [9], Monte Carlo ray tracing [10], the zone method [11], the spectral method [12] etc. The DOM solves the Radiative Transfer Equation (RTE) in differential form and requires various approximations to deal with the directionality of radiation transport or the spatial variations of radiative intensities along propagation paths. Therefore, the orthogonal schemes for selecting the various discrete directions of propagation of the radiative energy are essential. Carlson and Lee proposed the level symmetric quadrature for the application of the DOM in 3D geometries [13]. Until now, this quadrature set is still among the most widely used in three-dimensional DOM calculations. However, this scheme is known to yield negative and physically unrealistic weights at high quadrature orders.

In recent years, a number of new quadrature schemes have been developed. Comparative studies dedicated to the analysis of the performance of these quadrature schemes for radiative transfer simulations, for example, analysis in [14, 15], have also been conducted. However, most of these studies have focused on high-temperature combustion problems. In urban-scale radiation simulation, the geometrical and directional configurations are quite different. The present paper compares the overall performance(accuracy, flexibility in the choice of the number of directions, etc.) of various angular quadrature schemes in a representative set of test urban configurations for radiative transfer.

2. The Discrete Ordinate Method

2.1. The Radiative Transfer Equation (RTE)

The Radiative Transfer Equation is the fundamental relationship in radiative transfer in participating media. It describes how radiative intensities (defined as the radiative energy flow per unit area normal to the direction of the rays, unit solid angle, and unit wavelength) evolve as it propagates within the medium due to the interactions between the radiation field and the propagation

medium. It is written as follows:

$$\Omega.\nabla I_\lambda(s,\Omega) = -\beta_\lambda I_\lambda(s,\Omega) + \kappa_\lambda I^0_\lambda\left[T(s)\right] + \frac{\sigma_\lambda}{4\pi}\int_{\Omega'} P(\Omega,\Omega')I_\lambda(s,\Omega')d\Omega' \tag{1}$$

where $I_\lambda(s,\Omega)$ is the spectral (at wavelength λ) radiative intensity in the direction of propagation of the radiation field Ω and at a location s along a path in this direction Ω. I^0_λ is the local radiative emission given by the Planck law of blackbody intensity at the local temperature of the medium $T(s)$ (the assumption of local thermodynamical equilibrium here is reasonable). β_λ is the spectral extinction coefficient of the medium, which is the sum of the absorption κ_λ and scattering σ_λ coefficients. $P(\Omega,\Omega')$ is the phase function that describes the scattering of some incoming radiation represented by the intensity $I_\lambda(s,\Omega')$ from the direction Ω' to the new direction Ω.

In solving the boundaries of the computational domain of the RTE(walls, sky, etc), Eq. 1 is subject to the boundary condition:

$$I_\lambda(w,\Omega) = \epsilon_{w,\lambda}I_{b,w,\lambda} + \frac{1-\epsilon_{w,\lambda}}{\pi}\int_{\vec{n}.\vec{\Omega}<0} |\vec{n}.\vec{\Omega'}|.I_{w,\lambda}(\Omega')\,d\Omega' \tag{2}$$

In the previous equation, $\epsilon_{w,\lambda}$ is the spectral (at wavelength λ) emissivity of the boundary surface, $I_{b,w,\lambda}$ the blackbody intensity evaluated at the temperature of the surface element w, $\vec{n}$ is the normal to the surface at location w.

Because of the complexity of the urban surface, the calculation of scattering could consume too much time. For this reason, the atmosphere scattering is excluded from this paper. From now on, we will restrict the analysis to non-scattering media (σ_λ=0). In this case, the RTE is simplified into:

$$\Omega.\nabla I_\lambda(s,\Omega) = -\kappa_\lambda I_\lambda(s,\Omega) + \kappa_\lambda I^0_\lambda\left[T(s)\right] \tag{3}$$

2.2. *The Discrete Ordinate Method*

The Discrete Ordinate Method is one of the most prevalent techniques used to solve the RTE in participating media. This technique treats the RTE by using separate discretization schemes on space (ds) and angles (Ω). For this purpose, an angular discretization of variable Ω is used. This requires the selection of a quadrature set to evaluate numerically integrals over angles. Once this set has been chosen, for one single discrete direction Ω_m (characterized by a triplet of directional coefficients μ_m, η_m, ξ_m), the RTE is simplified into:

$$\Omega_m.\nabla I_\lambda(s,\Omega_m) = -\kappa_\lambda I_\lambda(s,\Omega_m) + \kappa_\lambda I^0_\lambda\left[T(s)\right] \tag{4}$$

In the case of a Cartesian spatial mesh, as covered in this work, the previous equation becomes:

$$\mu_m\frac{\partial I_\lambda(s,\Omega_m)}{\partial x} + \eta_m\frac{\partial I_\lambda(s,\Omega_m)}{\partial y} + \xi_m\frac{\partial I_\lambda(s,\Omega_m)}{\partial z} + \kappa_\lambda I_\lambda(s,\Omega_m) = \kappa_\lambda I^0_\lambda\left[T(s)\right] \tag{5}$$

where ∂x, ∂y, ∂z are local path increments that characterize the mesh over which the RTE is being solved.

The previous equation can be integrated over a single Cartesian cell (as depicted in Figure 1). In the general case, for a given choice of the direction of propagation Ω_m, the intensity at three interfaces of the cell is known at a given step of the propagation scheme (e.g., for instance, S_{left}, S_{bottom}, S_{front} are known as the incoming interfaces.) This provides the following discrete form:

$$\begin{aligned} S_{\lambda,p}\delta v = \mu_m Ax(I_{\lambda,S_{right},m} - I_{\lambda,S_{left},m}) + \eta_m Ay(I_{\lambda,S_{back},m} - I_{\lambda,S_{front},m}) \\ +\xi_m Az(I_{\lambda,S_{top},m} - I_{\lambda,S_{bottom},m}) + \kappa_\lambda I_{\lambda,p,m}\delta v \end{aligned} \tag{6}$$

Where the intensities $I_{\lambda,S,m}$ represent the interface averaged radiative intensities and we have

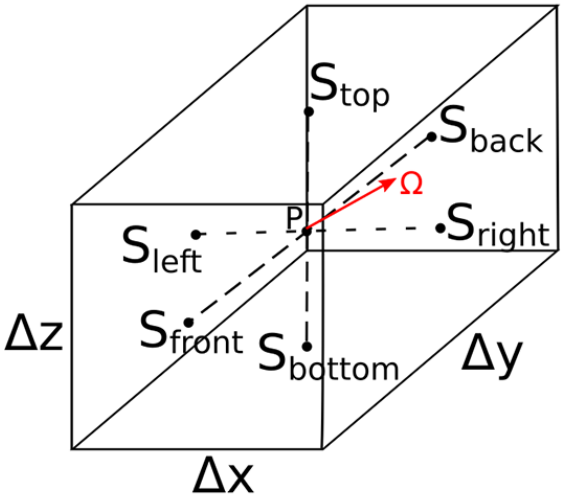

Figure 1: Cartesian cell considered in the Discrete Ordinate Method

used the notations:

$$\begin{aligned} Ax &= \Delta y \times \Delta z \\ Ay &= \Delta x \times \Delta z \\ Az &= \Delta x \times \Delta y \\ \delta v &= \Delta x \times \Delta y \times \Delta z \\ S_{\lambda,p} &= \kappa_\lambda I_\lambda^0 \left[T(s)\right] \end{aligned} \tag{7}$$

The intensities on the other three interfaces of the cell (S_{right}, S_{top}, S_{back}) can be obtained by introducing assumptions between the radiation intensity values on these interfaces and the volume average radiative intensity $I_{\lambda,p,m}$. These relationships usually take the form of linear interpolations (where α is a coefficient that may depend on the optical size of the cell in each dimension - its main constraint is to be between 0 and 1 although most usual values restrict its range of variation

to between 1/2 and 1):

$$\begin{aligned} I_{\lambda,p,m} &= I_{\lambda,S_{left},m} + \alpha(I_{\lambda,S_{right},m} - I_{\lambda,S_{left},m}) \\ &= I_{\lambda,S_{front},m} + \alpha(I_{\lambda,S_{back},m} - I_{S_{\lambda,front,m}}) \\ &= I_{\lambda,S_{bottom},m} + \alpha(I_{\lambda,S_{top},m} - I_{\lambda,S_{bottom},m}) \end{aligned} \tag{8}$$

Together with the previous set of relations, the following equation for the radiation intensity can eventually be obtained (assuming the same value of α for the three directions):

$$\begin{aligned} I_{\lambda,p,m} = \frac{\Lambda_{x,m} I_{\lambda,S_{left},m} + \Lambda_{y,m} I_{lambda,S,m} + \Lambda_{z,m} I_{\lambda,S_{bottom},m} + S_{\lambda,p} dv}{\Lambda_{x,m} + \Lambda_{y,m} + \Lambda_{z,m} + \kappa_\lambda \delta v} \\ \Lambda_{x,m} = \frac{\mu_m A x}{\alpha} \\ \Lambda_{y,m} = \frac{\eta_m A y}{\alpha} \\ \Lambda_{z,m} = \frac{\xi_m A z}{\alpha} \end{aligned} \tag{9}$$

Then, using the linear approximations set by Eq. 8, estimates of the unknown radiative intensities at the interface of the cell can be produced. The process is iterated over the whole mesh. The iteration ends when the maximum difference in intensity values between two successive iterations is reduced to a predetermined threshold.

3. Spatial differencing schemes

In this paper, we applied the hybrid interpolation scheme introduced by F. Liu, H. A. Becker, and A. Pollard in [16]. It consists of the definition of an interpolating coefficient α that depends on the chosen direction Ω_m through the following set of relationships:

$$\begin{aligned} \zeta_x^m &= max(0.5, \zeta_x^{m'}) \\ \zeta_y^m &= max(0.5, \zeta_y^{m'}) \\ \zeta_z^m &= max(0.5, \zeta_z^{m'}) \end{aligned} \tag{10}$$

where:

$$\begin{aligned}\zeta_x^{m'} &= 1 - \frac{a}{2 \times (b+c) + \kappa_\lambda} \\ \zeta_y^{m'} &= 1 - \frac{b}{2 \times (a+c) + \kappa_\lambda} \\ \zeta_z^{m'} &= 1 - \frac{c}{2 \times (a+b) + \kappa_\lambda}\end{aligned} \tag{11}$$

with:

$$\begin{aligned}a &= \frac{\mu_m}{\Delta x} \\ b &= \frac{\eta_m}{\Delta y} \\ c &= \frac{\xi_m}{\Delta z}\end{aligned} \tag{12}$$

This scheme performs better than the upwind ($\alpha = 1$) and centered ($\alpha = 0.5$) schemes. The only disadvantage compared to the other two methods is that it is more computationally demanding as it requires additional calculations related to the use of the previous set of relationships to define direction-dependent interpolating coefficients.

4. Angular quadrature schemes

Numerical quadrature formulas allow the integration of functions using a finite number of ordinates and their corresponding weights. According to [9, 17, 18], the constraints that generate the relevant quadrature for directional integration are:

- The discrete ordinate $\Omega_m(\mu_m, \eta_m, \xi_m)$ must be located on the unit sphere.

$$\mu_m^2 + \eta_m^2 + \xi_m^2 = 1 \tag{13}$$

- The weight factors must be positive and the zeroth moment condition should be ensured:

$$\sum_{m=1}^{n} \omega_m = 4\pi \tag{14}$$

- The number of photons (also known as the first moment condition) should be preserved which requires:

$$\sum_{m=1}^{n} \omega_m . \vec{\Omega}_m = 0 \tag{15}$$

- The diffusion condition (also referred to the second moment condition) should be satisfied and with δ the unit tensor can be seen as:

$$\sum_{m=1}^{n} \omega_m . \vec{\Omega}_m^2 = \frac{4\pi}{3}\delta \tag{16}$$

In addition, Lee[19], Carlson [8] and Truelove [20] proposed a half-moment first condition to calculate the unidirectional radiation flux at a wall. This condition can be expressed as:

$$\int_{\vec{\Omega}.\vec{n}<0} |\vec{\Omega}.\vec{n}| d\Omega = \int_{\vec{\Omega}.\vec{n}>0} \vec{\Omega}.\vec{n} d\Omega = \sum_{\vec{\Omega}.\vec{n}>0} \omega_m . \vec{\Omega}_m = \pi \tag{17}$$

In a more general frame, the quadrature should also satisfy as many moments as required to integrate accurately the phase function if the scattering of the radiant energy is non-isotropic in the practical heat transfer applications [21].

It can be noticed that discretization with a finite number of directions is almost impossible to satisfy the last constraint [18].

Most angular quadrature schemes were initially developed to solve problems in neutron transport theory [13, 8]. In the last decades, these schemes have also been adopted [22] and extended [21] to solve the RTE. Some quadratures were also designed to solve purely mathematical problems (i.e. based on some geometric considerations). Parts of the existing quadratures (some of which

are considered below) do not satisfy some of the constraints mentioned above but are still able to provide acceptable accuracy for radiative transfer calculations.

*4.1. **Level symmetric quadrature sets***

This quadrature is referred to as the S_N method and was developed by K. D. Lathrop and B. G. Carlson [23]. It provides directions that are symmetric with respect to a $\pi/2$ rotation inside eight octants. If one direction vector (μ, η, ξ) is chosen, then the different plus-minus signs of the other seven combinations of the same μ, η, ξ are also elements of the quadrature set. The main formula to evaluate the cosine values of the points on the unit sphere is:

$$\mu_m^2 = \mu_1^2 + 2(m-1)\frac{1-3\mu_1^2}{n-1} \qquad m = 1...n \tag{18}$$

The first base point μ_1 can be determined by Eq. (18) together with the constraint:

$$\sum_{m=1}^{\frac{n}{2}} \omega_m \mu^k = \frac{1}{k+1} \tag{19}$$

Basically, μ_1 is chosen by selecting which moment conditions need to be contented[8, 21]. Level symmetric quadratures can be categorized into 3 classes of quadrature:

- Level Symmetric Even quadrature (LSE): (19) in which the value of k is an even integer to satisfy the even moment conditions. This quadrature restricts n to be lower than 22 to avoid negative weights [15].
- Level Symmetric Odd quadrature (LSO): the value k is any positive integer. In contrast to the LSH described below, the LSO yields negative weights when $n \geqslant 12$.
- Level Symmetric Hybrid quadrature (LSH): the value k is chosen among the sequence $(0, 1, 2, 4, 6, n-2)$. It also restricts the maximum value of n to 10 to avoid negative weights.

In this paper, the S6 of the three types of Level Symmetric quadratures described above are considered and compared. The different directions and their corresponding weights in each quadrature set are listed in the Table 1:

Level Symmetric Even quadrature(LSE)			
n	Moments (k)	μ_m	Point weight
48(S6)	0 2 4 6	0.2666355 0.6815076 0.9261808	0.2766681 0.2469424
Level Symmetric Odd quadrature(LSO)			
n	Moments (k)	μ_m	Point weight
48(S6)	0 1 2 3	0.1838670 0.690514 0.9656013	0.1609518 0.3626469
Level Symmetric Hybrid quadrature(LSH)			
n	Moments (k)	μ_m	Point weight
48(S6)	0 1 2 4	0.1914858 0.6940220 0.9626351	0.1780147 0.3455840

Table 1: Table of S6 versions of quadrature LSE, LSO and LSH, with the different moment condition satisfied by the quadrature (Eq 19), the direction vectors and the corresponding point weights

*4.2. **Double Cyclic Triangles quadrature schemes***

In order to satisfy more moment conditions, the Double Cyclic Triangles have been proposed to increase the number of degrees of freedom [17]. The scheme is built on the superposition of non-degenerated and degenerated tuples of discrete ordinate in one octant. The arrangement of the zeroth level consists of six nodal points constructed with the help of the ordinate of one base point (μ, η, ξ). The initially generated levels assume that two of the directional cosines μ, η, ξ are the same, which transforms the arrangement into a latitudinal triangle. If all three ordinates share the same value, the DCT arrangement becomes a nodal point located in the center of the octant, which is the second generated level. The degrees of freedom corresponding to the three tuples are provided in Table 2.

The convention $DCTxyz_{abcd}$ has commonly been employed to designate such a quadrature scheme. The parameters x, y, z give the number of degenerate angles per level used in this ar-

Level of degeneration	Number of points	Degree of freedom
0	6	4
1	3	3
2	1	1

Table 2: Different levels of arrangement in DCT scheme

rangement, and the indices $a,\ b,\ c,\ d$ indicate the moment conditions contented by the quadrature. In this paper, we used the $DCT020$ schemes which contain $DCT020_{1246}$ and $DCT020_{2468}$. These two DCT schemes are similar respectively to the S6 scheme presented in the Level symmetric quadrature. The corresponding ordinates are provided in Table 3.

$DCT020$				
	μ_m	η_m	ξ_m	Point weight
$DCT020_{1246}$	0.13146076	0.13146076	0.98256609	0.16811011
	0.25166076	0.68434890	0.68434890	0.35548864
$DCT020_{2468}$	0.24154201	0.24154201	0.93984834	0.24375312
	0.26524016	0.68177989	0.68177989	0.27984562

Table 3: Table of $DCT020$

*4.3. **Equal weight quadrature schemes***

Based on his own LS scheme, Carlson developed an equal weight (EW) quadrature to treat neutron transport problems [24]. The scheme in this paper differs from LS in that there is no directional bias affecting the weights, which are:

$$\omega_m = \frac{\pi}{2}[\frac{n(n+2)}{8}]^{-1} \tag{20}$$

This scheme has been adopted to calculate radiation transfer problems [21], and its main difference from the LS scheme lies in the fact that the equal-weight scheme is not a latitude-based calculation. The tuples of ordinate are independent of each other. The satisfaction of the different moment conditions is controlled by a proper selection of these tuples. According to Fiveland [21], the direction vectors can be determined by different moment conditions written as:

$$\omega_m \sum_{m=1}^{\frac{n(n+2)}{8}} \mu^k = \frac{\pi}{2}\frac{1}{k+1} \tag{21}$$

In this paper, the Equal Weight Even (EWE) and Equal Weight Odd (EWO) quadratures as shown in Tables 4 are employed..

Equal Weight Even (EWE)			
n	Moments (k)	μ_m	Point weight
48(E6)	0 2 4 6	0.2561428 0.2663445 0.6815646 0.9320846	0.2617994
Equal Weight Odd (EWO)			
n	Moments (k)	μ_m	Point weight
48(E6)	0 1 2 3	0.2958759 0.0917517 0.7041241 0.9082483	0.2617994

Table 4: Table of E6 in the equal weight quadrature, with the different moment condition satisfied(eq 21), the direction vectors and the corresponded point weights

*4.4. **Constant weights for discrete ordinate methods (CWDOM)***

This quadrature set was developed by Taoufik Gassoumi and Rachid Said [25], which is an extension of the S_N method in which all the directions are given the same weights. Using the same notations as for the S_N quadrature of the previous section, the number of directions in one octant is with this new scheme equal to $\frac{n(n+1)}{2}$. The corresponding weights, assumed to be independent of the directions, are:

$$\omega_m = \frac{\frac{\pi}{2}}{\frac{n(n+1)}{2}} = \frac{\pi}{n(n+1)} \tag{22}$$

The coordinates of the directions are then given as:

$$\begin{aligned}
\mu_m &= \sin\theta_m \cos\phi_z = \sqrt{1-\xi_m^2}\cos\phi_z \\
\eta_m &= \sin\theta_m \sin\phi_z = \sqrt{1-\xi_m^2}\sin\phi_z \\
\xi_m &= \cos\theta_m = 1 - \frac{m^2}{n(n+1)} \\
d\phi &= \frac{\pi}{2n} \\
\phi_0 &= -\frac{d\phi}{2} \\
\phi_z &= \phi_{z-1} + d\phi
\end{aligned} \tag{23}$$

θ and ϕ are the azimuthal and polar angles in spherical coordinates. i and z vary from 1 to n. The CWDOM quadrature is also one of the quadrature set based on the S_N method and this indicates that the scheme is symmetric to any axis and it satisfies the zeroth, first and second moment conditions as in the LSO scheme.

4.5. ***The Tn sets***

Unlike the previously discussed quadrature schemes, these schemes were introduced to treat problems encountered in neutron transport theory. The Tn quadrature set [26] is one of the many methods based on geometric considerations.

This scheme bisects the surface of a triangle surface with vertices $(1,0,0)$,$(0,1,0)$,$(0,0,1)$ in the first octant. The ordinate of the vertices and centers of the small triangles are projected onto the unit sphere. The projection point of each smaller triangle center $(x_{tri},\, y_{tri},\, z_{tri})$ is used as the discrete ordinate with the relationship:

$$\begin{aligned}
\mu_m &= \frac{x_{tri}}{\sqrt{x_{tri}^2 + y_{tri}^2 + z_{tri}^2}} \\
\eta_m &= \frac{y_{tri}}{\sqrt{x_{tri}^2 + y_{tri}^2 + z_{tri}^2}} \\
\xi_m &= \frac{z_{tri}}{\sqrt{x_{tri}^2 + y_{tri}^2 + z_{tri}^2}}
\end{aligned} \tag{24}$$

The weight of each discrete direction is determined by the area of the outward spherical triangle projected on each small triangle. The Tn quadrature scheme has the disadvantage that there is no degree of freedom in the direction and weight factors to satisfy different moment conditions. The Tn quadrature can only provide directions that satisfy the zeroth and second moment conditions. The advantage is that this scheme is not limited by the number of discrete directions, which could yield the negative weight problem in some quadratures based on neutron theory like SN.

*4.6. **Spherical Rings Arithmetic Progression***

The Spherical Rings Arithmetic Progression(SARPN) [27] shares a similarity with the Tn sets. Both of them are based on geometric construction. Unlike the Tn sets, the SARPN divides directly the crown in one octant. As shown in Fig2, the crown is divided into several rings from top to bottom. Furthermore, each ring is separated into different elements which have an equal solid angle. The number of elements in the successive ring follows an arithmetic sequence that starts at 2 and adds 1 to each ring. The weight of each direction is the same.

The determination of discrete direction starts by calculating the centroid $(x_{SA},\, y_{SA},\, z_{SA})$ of the solid angle:

$$\begin{aligned} x_{SA} &= \frac{1}{V}\iiint\limits_{\Omega_m} x dV \\ y_{SA} &= \frac{1}{V}\iiint\limits_{\Omega_m} y dV \\ z_{SA} &= \frac{1}{V}\iiint\limits_{\Omega_m} z dV \end{aligned} \tag{25}$$

Then the coordinates of direction could be determined with:

$$\begin{aligned} \mu_m &= \frac{x_{SA}}{\sqrt{x_{SA}^2 + y_{SA}^2 + z_{SA}^2}} \\ \eta_m &= \frac{y_{SA}}{\sqrt{x_{SA}^2 + y_{SA}^2 + z_{SA}^2}} \\ \xi_m &= \frac{z_{SA}}{\sqrt{x_{SA}^2 + y_{SA}^2 + z_{SA}^2}} \end{aligned} \tag{26}$$

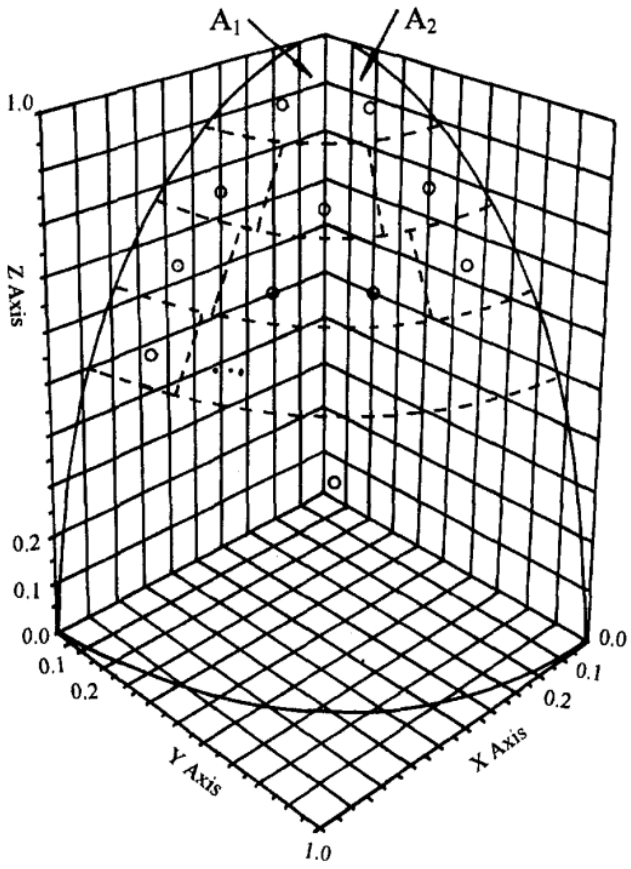

Figure 2: The SARPN schema [27]

4.7. ***The Fibonacci sets***

This distribution of points is founded on spherical Fibonacci lattices [28] [29] [30], which are defined as:

$$\begin{aligned} \theta_m &= \arccos(1 - \frac{2m}{F_m}) \\ \phi_m &= 2\pi m \frac{F_{m-1}}{F_m} \end{aligned} \tag{27}$$

where (θ_m, ϕ_m) are the angular coordinates of the i_{th} points of the quadrature in range of $[1, n]$

and F_m is the m_{th} Fibonacci number. F_m can be obtained as solution of the sequence:

$$\begin{aligned} F_0 &= 0 \\ F_1 &= 1 \\ F_m &= F_{m-1} + F_{m-2} \end{aligned} \tag{28}$$

With increasing m, the ratio $\frac{F_m}{F_{m-1}}$ converges quickly toward the golden ratio ϕ_{golden}. This provides the generator:

$$\begin{aligned} \theta_m &= \arccos(1 - \frac{2m}{n}) \\ \phi_m &= 2\pi m \phi_{golden}^{-1} \end{aligned} \tag{29}$$

Swinbank and Purser [31] improved this set by introducing an offset equal to $\frac{1}{N}$ on the z coordinate. This gives the so-called Spherical Fibonacci point sets:

$$\begin{aligned} \theta_m &= \arccos(1 - \frac{2m+1}{n}) \\ \phi_m &= 2\pi m \phi_{golden}^{-1} \end{aligned} \tag{30}$$

The Fibonacci quadrature satisfies only the zeroth moment condition as the weight factors of each discrete direction are equal. It can satisfy the first moment condition with a huge number of directions. But the higher moment condition can not be satisfied no matter how many directions there are. Also, this scheme is not symmetric like other schemes introduced in the previous sections.

4.8. ***The quasi Monte Carlo (QMC) sets***

Quasi-Monte Carlo methods are similar to Monte Carlo methods [32], except that instead of relying on (pseudo-)random numbers to generate statistical events (location of absorption, scattering direction, etc), Low-Discrepancy Sequence (LDS) [33] are used in QMC.

If two random numbers $(R_{\theta_m}, R_{\phi_m})$ are sampled in Monte Carlo from a uniform distribution within the interval $[0, 1]$, a point on the unit sphere can be defined. Its angular coordinates are given

by the following equation:

$$\begin{aligned} \theta_m &= \arcsin(\sqrt{R_{\theta_m}}) \\ \phi_m &= 2\pi R_{\phi_m} \end{aligned} \tag{31}$$

The same idea can be adopted for QMC by simply replacing the random numbers with elements of a Low-Discrepancy Sequence. LDSs are constructed in such a way that they map the unit hypercube more uniformly than random numbers and therefore converge faster than Monte Carlo methods for the calculation of integrals over $[0,1]^n$. In the present work, the LDS by Halton[34] has been chosen. Based on [35], the coordinates of the quadrature points on the unit sphere, in this case, are given as:

$$\begin{aligned} \mu_m &= 2\cos(2\pi R_1)\sqrt{R_2 - R_2^2} \\ \eta_m &= 2\sin(2\pi R_1)\sqrt{R_2 - R_2^2} \\ \xi_m &= 1 - 2R_2 \end{aligned} \tag{32}$$

where R_1 and R_2 are two numbers from the LDS. It is noted that in QMC, the weights are equal in all directions, as in the standard Monte Carlo techniques. This means this scheme can satisfy the zeroth moment condition, however, it can not satisfy the higher moment condition and it is also not symmetric to any axis.

5. Urban radiation calculation

5.1. ***Introduction***

Urban radiation consists of two parts, that is, solar radiation and thermal infrared radiation because of the radiative emission by the various surfaces encountered in the problem such as walls and grounds.

5.1.1. Solar radiation

For a given surface, the short wave (mostly in the visible part of the spectrum) radiation (I_{sw}) can be calculated as:

$$I_{sw} = I_{dir} + I_{dif} + I_{ref} \tag{33}$$

I_{dir} is the solar radiation that emanates directly from the sun, and this part has the highest radiation intensity of all three terms. The solar beam reaches the surfaces in the sunlight direction. The ray casting method is frequently used to treat this component because it is well suited to highly directional phenomena.

I_{dif} refers to the fraction of the incident solar radiation that is scattered by the atmosphere. Gas molecules, aerosol, $etc.$ scatter a part of the incident I_{dir}. Eventually, a fraction of this scattered energy reaches the surfaces (walls, ground, etc).

I_{ref} is the component related to reflections by the surfaces and this part of the energy may be derived from all elements of the mesh(since its value depends on the reflectivities of the surfaces).

In this article, different directional quadrature schemes are used to perform the calculation and the results are compared and analyzed. To simplify the calculations, some assumptions are made as follows:

- We applied two different boundary conditions for the two different types of solar radiation. A periodic boundary condition is taken to treat the vertical surfaces in the direct solar part. If a ray with intensity I_{ray} hits a vertical surface at coordinates (x_p, y_p, z_p), then the intensity values are assumed to be the same at points $(0, y_p, z_p)$ in the same direction of propagation, as depicted in Figure 3. This method reduces the need for information on the vertical surfaces and simplifies the treatment of the radiative transfer problem. On the other hand, an isotropic sky model [36] is used in the diffused part to simplify the calculation and reduce the meteorological information requirement. The emissivity is uniform for all sky boundaries

- All surfaces in the model are Lambertian with perfect diffuse reflection. The surface albedo

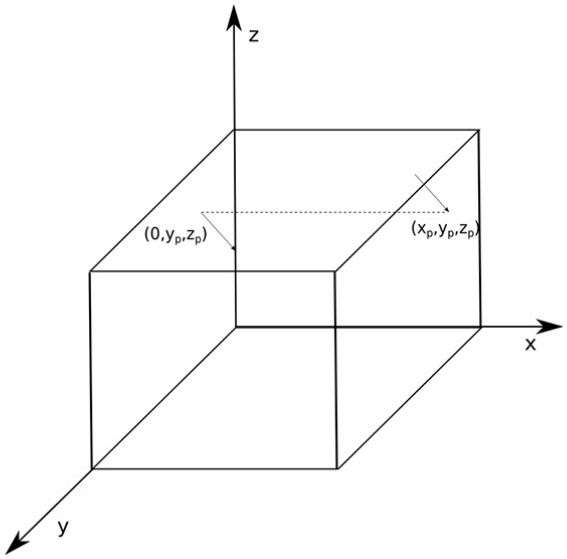

Figure 3: The periodic boundary condition

is gray and is not dependent on the wavenumber of the radiation, over each surface element. However, different surfaces may have distinct values of albedo.

- Simulating the direct solar radiation transfer with the DOM is performed in two steps:

  1: First the direct solar energy received by the surface without any reflection is calculated, so that only the part of radiation along the sun direction is considered. The focus of this step is to calculate the first impact of solar beams on the various boundaries (building, ground, etc). The specific choice of a quadrature set has no influence on this step, since only a single direction of propagation is considered. The quadrature will have an impact on the reflections on the scene calculated in the next step.

  2: Once this first calculation has been performed, it is possible to estimate the source terms associated with the direct solar energy reaching the various surfaces and to calculate the mutual reflection of the radiated beams on these surfaces. This second step is strongly dependent on the choice of the quadrature scheme used to evaluate the various directions of propagation of the reflected/emitted radiative intensities.

5.1.2. Infrared radiation

The thermal infrared radiation received by a surface is due to the sky I_{sky} and the environment I_{env} radiations. The amount of thermal infrared radiation from the sky is determined by its emissivity ϵ_{atm} and an effective temperature T_{atm} [37]. The environment radiation I_{env} corresponds to the component I_{ref} in solar radiation and accounts for radiative thermal emission by all boundary surface elements. Detailed information about the building geometries is significantly necessary for an accurate estimate of this component. Both parts, I_{sky} and I_{env}, are difficult to evaluate precisely in practice because of limited knowledge about wall and ground emissivities. They are often considered as Lambertian boundary surfaces with given prescribed temperatures and gray emissivities.

In this paper, all the sky surfaces are treated as diffuse with a prescribed temperature and emissivity. The bottom surfaces representing the ground are modeled also as diffuse with their own temperature and emissivity. In the next section, the performance of the quadrature method is evaluated in a typical geometry representative of the urban area, namely, the canyon.

5.2. ***Model Presentation***

In the urban radiation transfer field, it is hard to find a benchmark problem with an exact analytical solution as in other fields[38, 39]. In order to evaluate the quadratures' performances, a canyon, which can be seen as the basic component of city configurations, is studied. The calculated parameters including distances and heights are shown in figure 4.

The other boundary conditions for solar radiation are given in table 5,while the IR radiation is presented in Table 6.

The incident heat fluxes on each surface were calculated in both solar and infrared regimes. The same calculation was also carried out with the finite volume method, which had been already verified by a benchmark problem calculation [40]. Three comparisons have been realized by this paper:

- Based case: The space was discretized into identical cubes with a dimension of 1 m in each direction. All the quadratures presented in the previous sections were evaluated: LS (LSO,

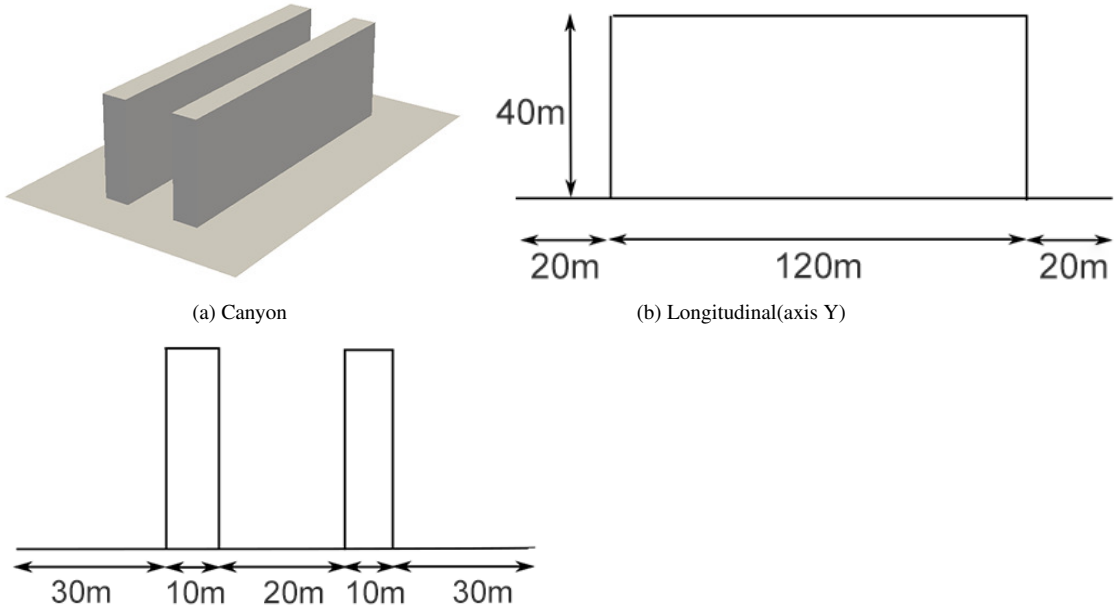

(a) Canyon

(b) Longitudinal(axis Y)

(c) Transversal(axis X)

Figure 4: Model for the solar radiation calculation

Soil emissivity	0.95
Wall emissivity	0.91
Roof emissivity	0.88
Sky absorbility	1
Azimuth angle	43.8983°
Elevation angle	62.3438°
Sun direction	(0.3218,0.3348,-0.8857)
Direct solar radiation received by horizontal surface	842.2396 W/m^2
Diffused solar radiation received by horizontal surface	102.3310 W/m^2

Table 5: Boundary condition for solar radiation test - Canyon geometry of Figure 4

LSE, LSH), EW (EWO, EWE), DCT, Fibonacci, QMC, CWDOM, Tn, and SARPN. The number of directions of all quadratures was fixed at 48 except Tn and SARPN. This is because of the principle of construction of quadratures, where Tn2 was selected here providing 32 discrete directions in the quadrature set and 40 for the quadrature SARPN. For the LS, EW, and DCT quadratures, the LS6, EW6 and, DCT020 were chosen and these quadratures satisfy different sets of moment conditions. The atmosphere in this case is considered a transparent medium.

- Spatial and angular refinement case: In this part, this paper refined the spatial and angular

Soil emissivity	0.95
Soil temperature	300K
Wall emissivity	0.91
Roof emissivity	0.88
Building temperature	285K
Sky absorbility	1
Sky temperature	273K

Table 6: Boundary condition for infrared radiation

discretization to evaluate the performance of quadrature in different kinds of mesh configurations. The mesh sizes in this section were set to 2m, 1m, and 0.5m, respectively. For the angular refinement, this paper increased the direction number from the previous case to 80 and 120. The direction numbers and quadratures used in this section are shown in Table7. The atmosphere is also considered a transparent medium.

- Atmosphere absorption case: Based on the previous case, the atmosphere is considered to be participative. A grey model has been applied with an absorption coefficient of $0.1m^{-1}$.

Direction number	Quadrature
32	TN2
40	SARP2
48	CWDOM DCT020-1 DCT020-2 EWE6 EWO6 FIBO QMC LSE6 LSO6 LSH6
72	TN3 SARP3
80	CWDOM DCT111-1 DCT111-2 EWE8 EWO8 FIBO QMC LSE8 LSO8 LSH8
112	SARP4
120	CWDOM FIBO QMC
128	TN4

Table 7: The directions number and the quadrature correspond

6. *Result analysis*

6.1. Based case

6.1.1. Solar radiation

The results of solar radiation simulations with FVM and DOM of the canyon geometry are depicted in Figure 5. These contain I_{dir}, I_{dif} and I_{ref} mentioned in the section 5.1.1. The results

given by the two methods are very similar. To determine the difference between the results, we calculated the MAE and RMSE for all building patches. These quantities are defined in Formula 34.

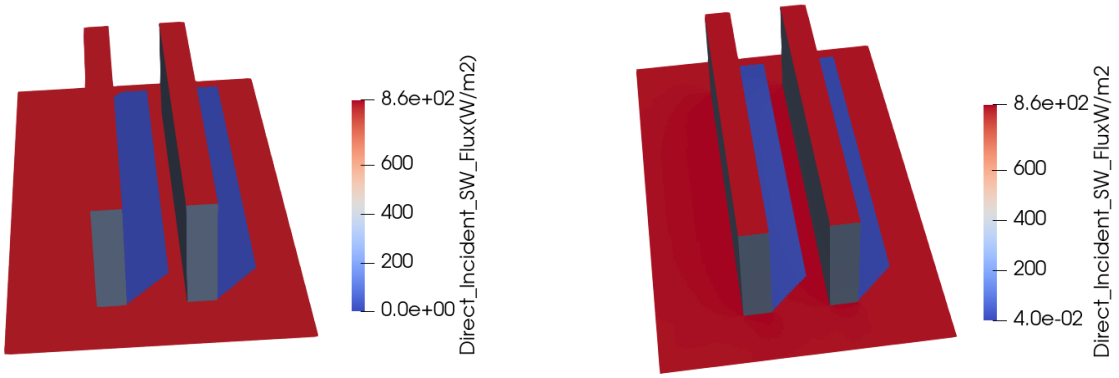

(a) FVM

(b) DOM:LSO6

Figure 5: Direct solar radiation received by the canyon surface, calculated by FVM and DOM(quadrature LSO6)

$$MAE = \frac{\sum^{patch\ number} |\phi_{DOM} - \phi_{FVM}|}{patch\ number}$$
$$RMSE = \sqrt{\frac{\sum^{patch\ number} (\phi_{DOM} - \phi_{FVM})^2}{patch\ number}} \tag{34}$$

The results of MAE and RMSE for all quadratures are plotted in Figure 6. The values reported in it only show slight differences among the various quadrature schemes. The Fibonacci quadrature performs the best among these schemes in this configuration even if it does not completely guarantee any moment condition other than the zeroth one. In the case of the QMC set, due to the small number of directions used for the calculations, poor performances are obtained compared with the other schemes considered. For the case of the study, 48 discrete directions are insufficient for QMC to get relatively accurate results. For the Tn scheme, even if it has a small number of directions, relatively good results are observed. At the same time, as a quadrature based on geometric consideration, the SARPN has a higher MAE and RMSE. Concerning the quadrature sets initially proposed in neutron transport theory, the DCT is worse than EW and LS, especially the DCT020-1. The differences between EW and LS are rather small.

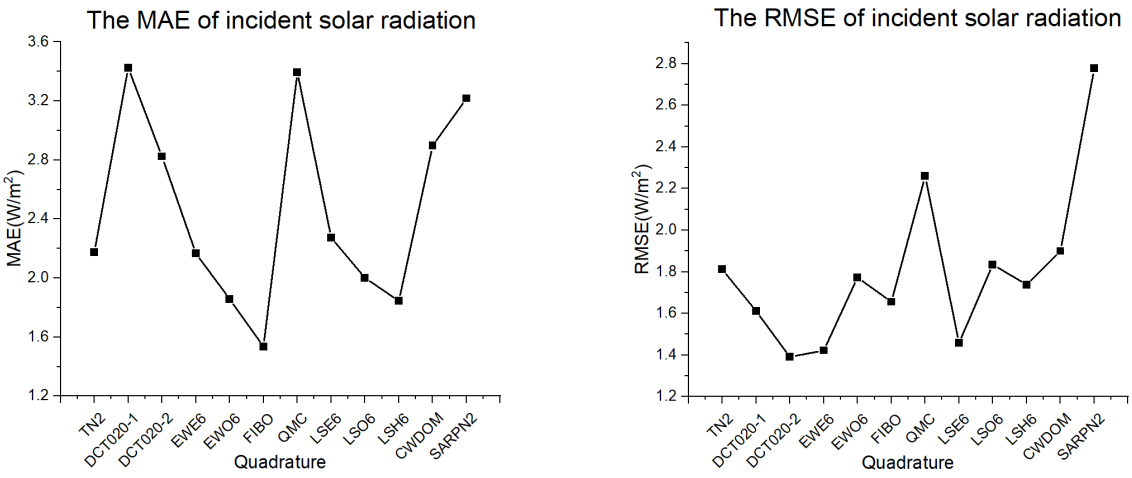

(a) MAE (b) RMSE

Figure 6: The difference of solar energy calculated by FVM and DOM with different quadrature schemes

6.1.2. Infrared radiation

On the side of the Infrared radiation, the result of incident flux on each patch are shown in Figure 7

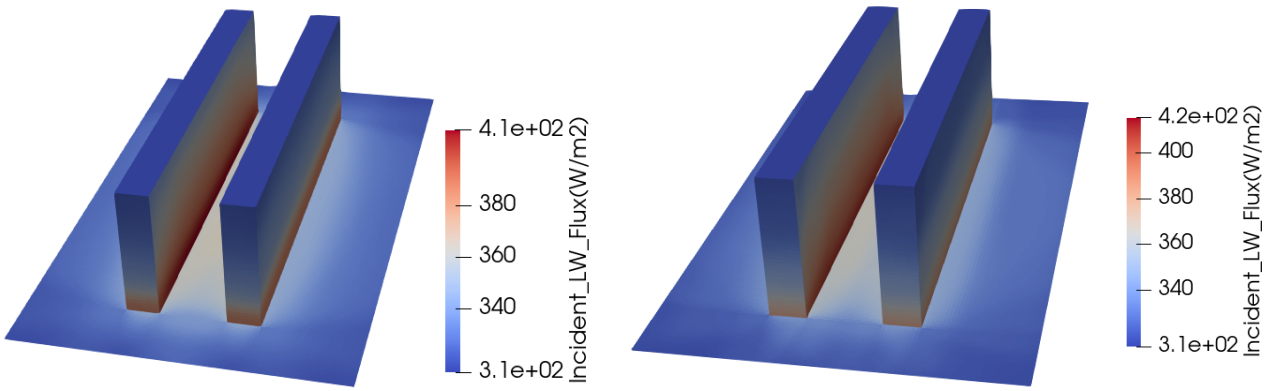

(a) FVM (b) LSO6

Figure 7: The incident infrared radiation on each patch with FVM and DOM(LSO6)

Herein, in the infrared, the sky boundary is no longer a dominant source of radiation because the temperature of the buildings and ground surfaces is higher than that of the sky. Owing to the short distances between the two infrared radiation sources (buildings and ground), the bottom of the walls receives more energy than other surfaces. This effect is amplified in the U-shape because of the inter-reflections between the walls.

The errors of the different quadrature schemes are illustrated in Figure8. In this configuration,

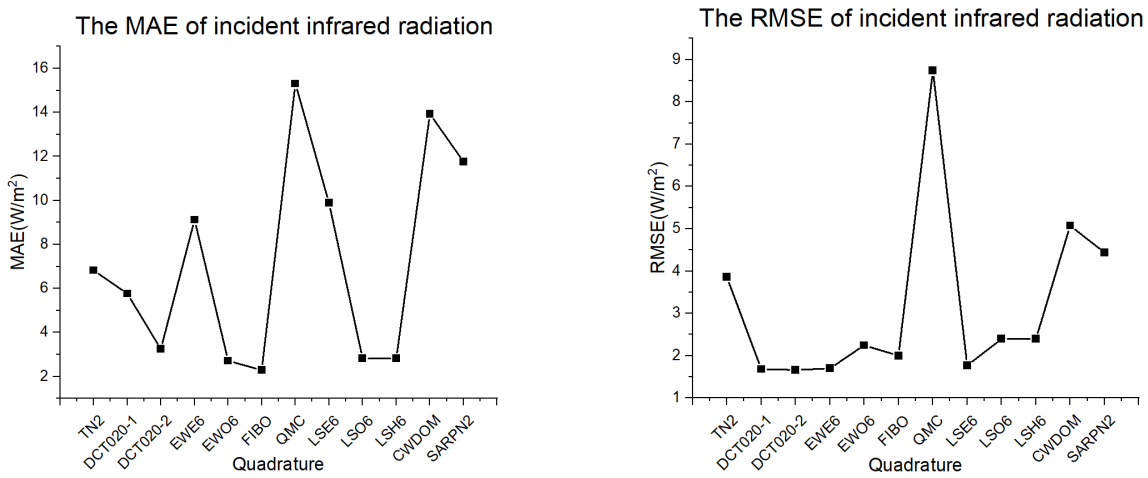

(a) MAE (b) RMSE

Figure 8: The difference of infrared radiation calculated by FVM and DOM with different quadrature schemes

differences up to $10W/m^2$ are observed for some quadratures. The RMSE of most quadratures increases compared with the values observed in solar radiation. This increase remains at about $1W/m^2$ in most cases. The Fibonacci set still provides the smallest MAE, closely followed by the $DCT020_{1246}$, EWO6, LSO6, and LSH6 schemes. The CWDOM performs poorly, as QMC, which requires obviously more discrete directions to ensure an acceptable quality of the calculations. Despite the disadvantage in the number of directions, the Tn2 quadrature still provides relatively good results. Despite a decline in RMSE, the SARPN schema still provides a relatively higher MAE. The insufficient direction number could be the reason.

This analysis of the based case confirms that the Fibonacci scheme is the most relevant choice among the studied configurations. It produces the smallest errors in all three cases of canyon calculations, even if it only obeys the zeroth moment condition. The DCT ($\text{DCT}020_{1246}$) and LS schemes (LSO6, LSH6) are also acceptable choices in this simulation. Compared with the Fibonacci scheme, these sets have a huge advantage that both are symmetric around the axis. This property is vital for the DOM to treat the specular reflections because the reflected directions are naturally contained in the quadrature scheme. However, due to the negative weight problem, the number of discretization is limited which may create problems if a higher order of quadrature is required.

6.2. *Spatial and angular refinement case*

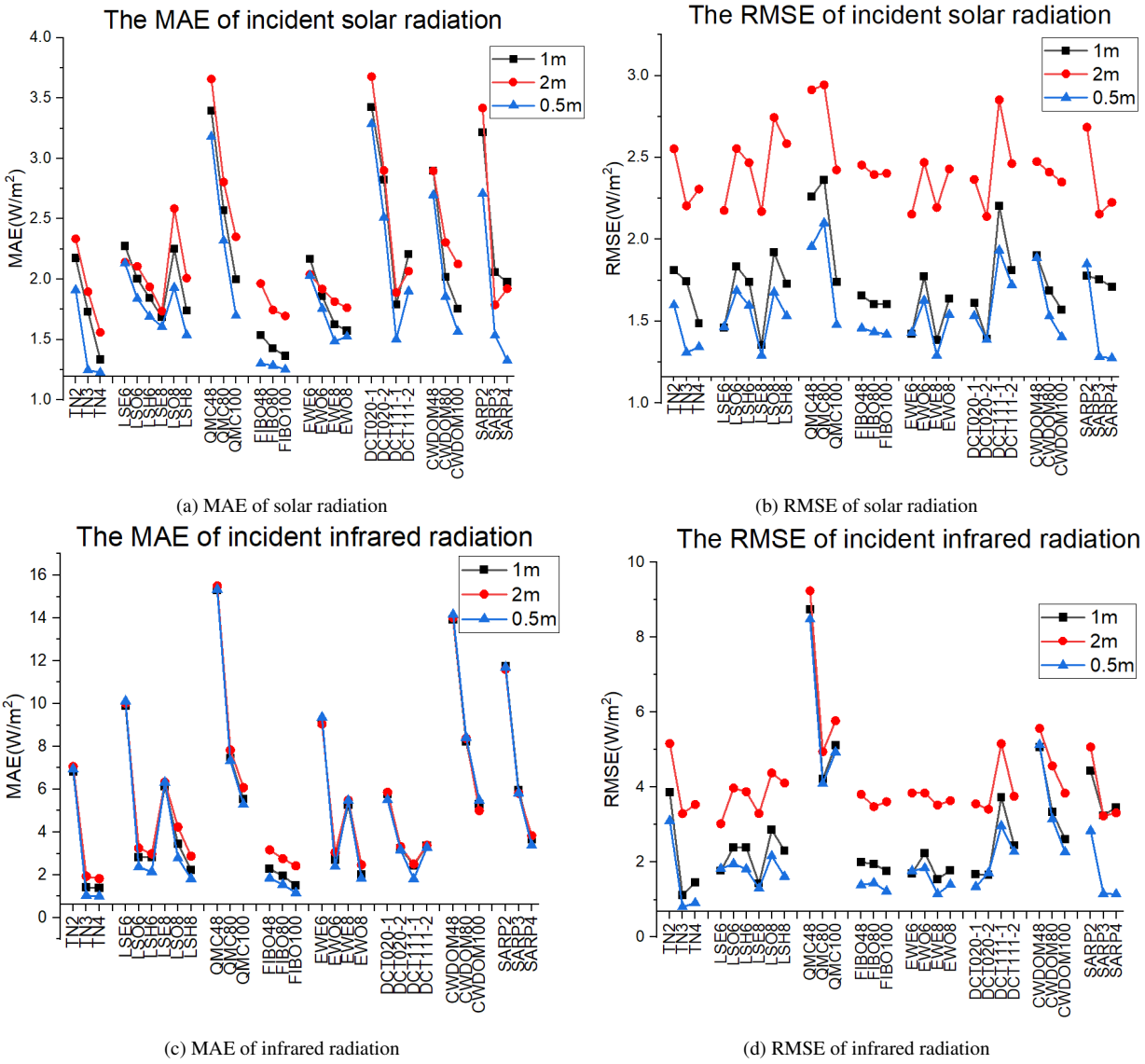

(a) MAE of solar radiation

(b) RMSE of solar radiation

(c) MAE of infrared radiation

(d) RMSE of infrared radiation

Figure 9: The results with spatial and angular refinements

The results of MAE and RMSE for both solar and infrared radiation can be found in the Figure 9 and analyzed in a manner of angular and spatial variation.

The influence of mesh refinement on both solar and infrared radiation is relatively small. The maximum error decrease is limited to $1W/m^2$. The result suggests that mesh refinement could barely optimize the MOD result in a canyon case. This conclusion favors the urban simulation with DOM because it does not need a refined mesh for good accuracy, which could largely reduce the

time consumption.

The angular refinement generates a greater influence on results. The rise of directions numbers reduces the difference between the DOM and FVM results. For quadratures CWDOM, QMC, DCT-1, TN and SARPN, the increase in discretization number can greatly improve their performances in the calculation of all types of radiations. The convergence of the Fibonacci quadrature stays at a very small quantity with a direction number beyond 48 in the calculation. This means the need for the directional discretization to obtain an accurate result by Fibonacci quadrature in this configuration could be much less than 48, leading to a big advantage for the Fibonacci quadrature in the manner of simulation time-saving.

Overall, it could be found that despite the improvement by spatial refinement with a fixed direction number, the increasing of angular discretization number is more efficient to reduce the difference, in particular to the CWDOM, QMC, DCT-1, TN and SARPN quadratures. The Fibonacci quadrature appears to slightly outperform other quadratures in this application, given that relative differences are lower when compared to other methods with increasing angular and spatial refinement. For the LS and EW quadrature, the results from odd and hybrid schemes are better than the even's.

6.3. Atmosphere absorption case

In this case, an atmosphere absorption coefficient $0.1m^{-1}$ is applied with the same configuration used in the Spatial and angular refinement case. Because solar radiation has been already absorbed during the passing through the atmosphere, the amount of absorption of solar radiation in the urban area could be very small. For this reason, only the infrared absorption was included in the calculation. The result is shown in Figure 10. The MAE curve does not change too much from the transparent case (Fig 9c). Most of the errors increase slightly with the absorption involved. The schemes of LSO, LSH, and EWO have a better MAE result than Fibonacci's with the same angular discretization. Only with 100 directions, the Fibonacci scheme could regain the title. For the RMSE result, most of schemes remain at a low level, except the QMC and CWDOM schemes. In conclusion, the LSO,LSH, and EWO schemes surpass the Fibonacci scheme in an atmosphere

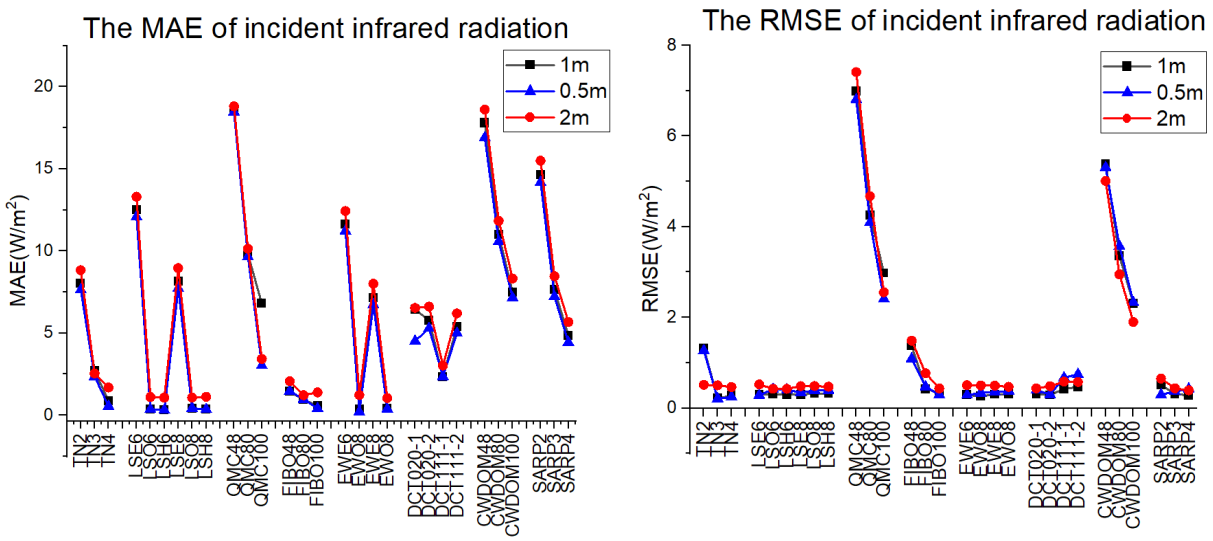

(a) MAE

(b) RMSE

Figure 10: The difference of infrared radiation calculated by FVM and DOM with an absorption atmosphere model

absorption case, but the disparity stays tiny. It should be noted that if the scattering is considered, this gap could increase as the schemes which satisfy more rigorous moment conditions are likely required to more accurately integrate the phase function.

7. Conclusion

This paper introduces, compares, and analyzes several quadrature schemes handling angular discretization in urban configurations. The main objective is to find a quadrature set providing accurate results with the smallest computational burden. Based on these results described in the paper, the Fibonacci quadrature set seems to be the best choice among the ones considered in the transparent case, since it provides accurate results even at very low orders, even if it does not satisfy most of the moment conditions. Besides, the best choice switches to LSO, LSH, and EWO while the atmosphere absorption is considered, but the Fibonacci scheme is also a good choicthe e in this case. In the aspect of quadrature structure, the Fibonacci scheme is more flex ible in direction choice, and it can keep a good accuracy with a relatively small direction number. For LSO, LSH, and EWO, the choices of direction numbers are few, but they can deal with the specular reflection because of their symmetric structure.

However, it is noticed that the quadrature scheme used to treat the angular dependency of radiative intensities is not the only important factor to be considered in accurate radiative transfer calculations at the city scale: spatial discretization, accurate treatments of gaseous / particles scattering, appropriate treatment of boundary conditions, etc., and it also has a significant impact on the outcome of the simulations. Some of these additional possible sources of errors include the current review as a continuation of the current work. At the same time, this paper used the FVM result to compare, a more precise simulation or measure result will be recommended in future study.

References

[1] B. Raybaud, P. Thony, E. Vergnault, L. Merlier, and J.-J. Roux, "Preliminary numerical evaluation of the bipv's potential in urban areas: Which method to use for solar radiation calculation?," 2020.

[2] D. Robinson and A. Stone, "Solar radiation modelling in the urban context," *Solar Energy*, vol. 77, no. 3, pp. 295 – 309, 2004.

[3] D. Robinson, N. Campbell, W. Gaiser, K. Kabel, A. Le-Mouel, N. Morel, J. Page, S. Stankovic, and A. Stone, "Suntool – a new modelling paradigm for simulating and optimising urban sustainability," *Solar Energy*, vol. 81, no. 9, pp. 1196 – 1211, 2007. CISBAT 2005.

[4] J. C. Chai, H. S. Lee, and S. V. Patankar, "Finite volume method for radiation heat transfer," *Journal of Thermophysics and Heat Transfer*, vol. 8, no. 3, pp. 419–425, 1994.

[5] P. J. Coelho, "Advances in the discrete ordinates and finite volume methods for the solution of radiative heat transfer problems in participating media," *Journal of Quantitative Spectroscopy and Radiative Transfer*, vol. 145, pp. 121–146, 2014.

[6] F. N. Çayan and N. Selçuk, "The method of lines solution of discrete ordinates method for non-grey media," *Journal of Quantitative Spectroscopy and Radiative Transfer*, vol. 104, no. 2, pp. 228–237, 2007.

[7] Y. Billaud, D. Saury, and D. Lemonnier, "Numerical investigation of coupled natural convection and radiation in a differentially heated cubic cavity filled with humid air. effects of the cavity size," *Numerical Heat Transfer, Part A: Applications*, vol. 72, pp. 1–24, 10 2017.

[8] B. Carlson and K. Lathrop, "Transport theory: The method of discrete ordinates," Tech. Rep. LA-4554, Los Alamos Scientific Lab., N. Mex. United States, 1965.

[9] M. F. Modest, "Chapter 16 - the method of discrete ordinates (sn-approximation)," in *Radiative Heat Transfer (Second Edition)* (M. F. Modest, ed.), pp. 498–538, Burlington: Amsterdam,NL.Elsevier, second edition ed., 2003.

[10] D. Stankevich and Y. Shkuratov, "Monte carlo ray-tracing simulation of light scattering in particulate media with optically contrast structure," *Journal of Quantitative Spectroscopy and Radiative Transfer*, vol. 87, no. 3, pp. 289–296, 2004.

[11] G. Xu and W.-Y. Duan, "Time-domain simulation of wave–structure interaction based on multi-transmitting formula coupled with damping zone method for radiation boundary condition," *Applied Ocean Research*, vol. 42, pp. 136–143, 2013.

[12] B.-W. Li, X.-H. Luo, and W. Wang, "Simulations of radiation hydrodynamics and radiative magnetohydrodynamics by collocation spectral methods," *Computers Fluids*, vol. 164, pp. 119–124, 2018. Special Issue devoted to The Asian Symposium on Computational Heat Transfer and Fluid Flow 2015 (ASCHT 2015) held in Busan, Korean on November 22-25, 2015.

[13] B. Carlson and C. Lee, "Mechanical quadrature and the transport equation," Tech. Rep. LAMS-2573, Los Alamos Scientific Lab., N. Mex. United States, 1961.

[14] X. Hu and Y. Y. Azmy, "Asymptotic convergence of the angular discretization error in the scalar flux computed from the particle transport equation with the method of discrete ordinates," *Annals of Nuclear Energy*, vol. 138, pp. 107–199, 2020.

[15] K. Manalo, C. D. Ahrens, and G. Sjoden, "Advanced quadratures for three-dimensional discrete ordinate transport simulations: A comparative study," *Annals of Nuclear Energy*, vol. 81, pp. 196–206, 2015.

[16] F. Liu, H. A. Becker, and A. Pollard, "Spatial differencing schemes of the discrete-ordinates method," *Numerical Heat Transfer, Part B: Fundamentals*, vol. 30, no. 1, pp. 23–43, 1996.

[17] R. Koch, W. Krebs, S. Wittig, and R. Viskanta, "Discrete ordinates quadrature schemes for multidimensional radiative transfer," *Journal of Quantitative Spectroscopy and Radiative Transfer*, vol. 53, no. 4, pp. 353–372, 1995.

[18] R. Koch and R. Becker, "Evaluation of quadrature schemes for the discrete ordinates method," *Journal of Quantitative Spectroscopy and Radiative Transfer*, vol. 84, no. 4, pp. 423–435, 2004.

[19] C. E. Lee, "The discrete sn approximation to transport theory," Tech. Rep. LA-2595, Los Alamos Scientific Lab., N. Mex. United States, 6 1961.

[20] J. S. Truelove, "Discrete-Ordinate Solutions of the Radiation Transport Equation," *Journal of Heat Transfer*, vol. 109, pp. 1048–1051, 11 1987.

[21] W. A. Fiveland, "The selection of discrete ordinate quadrature sets for anisotropic scattering," *Fundamantals of radiative heat transfer*, vol. 160, pp. 89–96, 1991.

[22] W. A. Fiveland, "Discrete-Ordinates Solutions of the Radiative Transport Equation for Rectangular Enclosures," *Journal of Heat Transfer*, vol. 106, pp. 699–706, 11 1984.

[23] K. D. Lathrop and B. G. Carlson, "Discrete ordinates angular quadrature of the neutron transport equation," Tech. Rep. LA-3186, Los Alamos Scientific Lab., N. Mex. United States, 9 1964.

[24] B. Carlson and L. A. S. Laboratory, "Tables of equal weight quadrature eqn over the unit sphere," Tech. Rep. LA-4734, Los Alamos Scientific Lab., N. Mex. United States, 1971.

[25] T. Gassoumi and R. Said, "Application of a new quadrature scheme for the discrete ordinate method to investigate radiative heat transfer in a spherical geometry," *Science Academy Transactions on Renewable Energy Systems Engineering and Technology*, vol. 1, pp. 59–67, June 2011.

[26] C. Thurgood, A. Pollard, and H. Becker, "The tn quadrature set for the discrete ordinates method," *Journal of Heat Transfer*, vol. 117, pp. 1068–1070, 11 1995.

[27] B.-W. Li, Q. Yao, X.-Y. Cao, and K.-F. Cen, "A New Discrete Ordinates Quadrature Scheme for Three-Dimensional Radiative Heat Transfer," *Journal of Heat Transfer*, vol. 120, pp. 514–518, 05 1998.

[28] J. Hannay and J. Nye, "Fibonacci numerical integration on a sphere," *Journal of Physics A: Mathematical and General*, vol. 37, pp. 11591–11601, 11 2004.

[29] R. Marques, C. Bouville, L. P. Santos, and K. Bouatouch, *Efficient Quadrature Rules for Illumination Integrals: From Quasi Monte Carlo to Bayesian Monte Carlo*. Morgan & Claypool, 2015.

[30] D. Svergun, "Solution scattering from biopolymers: Advanced contrast variation data analysis," *Acta Crystallographica Section A*, vol. 50, pp. 391–402, 05 1994.

[31] R. Swinbank and R. Purser, "Fibonacci grids: A novel approach to global modelling," *Quarterly Journal of the Royal Meteorological Society*, vol. 132, pp. 1769 – 1793, 02 2006.

[32] W. L. Dunn and J. K. Shultis, *Exploring Monte Carlo Methods*. Amsterdam,NL.Elsevier, 2012.

[33] C. Lemieux, *Monte Carlo and Quasi-Monte Carlo Sampling*. Springer Series in Statistics, New York, NY.USA.Springer, 2009.

[34] J. Halton, "On the efficiency of certain quasi-random sequences of points in evaluating multi-dimensional integrals," *Numerische Mathematik*, vol. 2, pp. 84–90, 1960.

[35] J. S. Brauchart and J. Dick, "Quasi-monte carlo rules for numerical integration over the unit sphere s^2," *Numerische Mathematik*, vol. 121, pp. 473–502, Jan. 2011.

[36] B. Y. Liu and R. C. Jordan, "The interrelationship and characteristic distribution of direct, diffuse and total solar radiation," *Solar Energy*, vol. 4, no. 3, pp. 1–19, 1960.

[37] T. M. Crawford and C. E. Duchon, "An Improved Parameterization for Estimating Effective Atmospheric Emissivity for Use in Calculating Daytime Downwelling Longwave Radiation," *Journal of Applied Meteorology*, vol. 38, pp. 474–480, 04 1999.

[38] R.-R. Zhou, B.-W. Li, and Y.-S. Sun, "Predicting radiative heat transfer in axisymmetric cylindrical enclosures using the collocation spectral method," *International Communications in Heat and Mass Transfer*, vol. 117, p. 104789, 2020.

[39] R.-R. Zhou, Y.-S. Sun, B.-W. Li, and J. Ma, "The composite chebyshev integration method for radiative integral transfer equations in rectangular enclosures," *International Journal of Thermal Sciences*, vol. 170, p. 107141, 2021.

[40] E. V. Félix Schmitt, Frederic Andre, "A cfd solver based on the lattice boltzmann method to solve three-dimensional thermally driven flows and coupled molecular gas radiation: Comparison and validation against a benchmark solution," in *Proceedings of the 7th Thermal and Fluids Engineering Conference*, pp. 409–418, 2022.